

Signatures of a subpopulation of hierarchical mergers in the GWTC-4 gravitational-wave dataset

Cailin Plunkett ^{1D*} and Salvatore Vitale ^{1D}

LIGO Laboratory, Massachusetts Institute of Technology, Cambridge, MA 02139, USA

Kavli Institute for Astrophysics and Space Research, Massachusetts Institute of Technology, Cambridge, MA 02139, USA and Department of Physics, Massachusetts Institute of Technology, Cambridge, MA 02139, USA

Thomas Callister ^{1D}

Williams College, Williamstown, MA 01267, USA

Michael Zevin ^{1D}

Adler Planetarium, 1300 South DuSable Lake Shore Drive, Chicago, IL, 60605, USA

Center for Interdisciplinary Exploration and Research in Astrophysics (CIERA),

Northwestern University, 1800 Sherman Avenue, Evanston, IL, 60201, USA and

NSF-Simons AI Institute for the Sky (SkAI), 172 East Chestnut Street, Chicago, IL, 60611, USA

(Society of Physicists Interested in Non-aligned Spins, SPINS)[†]

(Dated: January 14, 2026)

Repeated black-hole mergers in dense stellar clusters are a plausible mechanism to populate the predicted gap in black hole masses due to the pair-instability process. These hierarchical mergers carry distinct spin and tilt features relative to first-generation black holes, for which previous studies have found evidence at a population level by interpreting features in the effective inspiral spin domain. We introduce an astrophysically-motivated model in the joint space of effective inspiral and precessing spins, which captures the dominant spin dynamics expected for hierarchical mergers. We find decisive evidence both for a population transition above $\sim 45M_{\odot}$, consistent with the anticipated onset of the pair-instability gap, as well as a peak at $\sim 15M_{\odot}$, which we interpret as the global peak in the hierarchical merger rate. The existence of low- and high-mass subpopulations of higher-generation black holes suggests the contribution of both near-solar-metallicity and metal-poor star clusters to the hierarchical merger population. Our results reinforce the growing evidence for detailed, mass-dependent substructure in the spin distribution of the binary black hole population.

Introduction — Theoretical models for the formation of binary black holes (BBH) can be broadly divided into two classes: isolated evolution of field binary stars and dynamical channels [see, e.g., 1–3, for reviews]. Identifying the formation history of an individual merger can be difficult since multiple channels may be consistent with a given set of black-hole parameters. The latest catalog of gravitational-wave (GW) events [4, 5] released by the LIGO–Virgo–Kagra (LVK) collaboration [6–10] allows for the most detailed investigation yet of the constitution of the BBH population.

It is increasingly clear, both from individual events and population analyses, that massive black holes exist in the range $45\text{--}120M_{\odot}$ [11–14]. This is in tension with the notion of pair-instability supernovae (PISNe), which stellar evolution theory predicts should create a gap in this interval [15–23]. These unexpected observations have spurred further investigation into mechanisms that can populate this upper mass gap, one of which being hierarchical mergers [24–28].

Most observed BBH are thought to contain two first-generation black holes formed directly from stellar col-

lapse, resulting in a remnant second-generation black hole. In dense stellar environments, remnants may undergo subsequent coalescences, creating hierarchical mergers: those containing at least one component that is the product of one or more previous mergers [29–34]. Hierarchical mergers are characterized by higher primary masses, isotropic spin orientations [29], and dimensionless spins $\chi \approx 0.7$, arising from the remaining orbital angular momenta of their progenitors [35–39], with spread due to their mass ratio and spins [40, 41]. Since hierarchical assembly produces more massive black holes, it is a natural candidate for a method to fill the PISN gap. These predictions for spin and spin-tilt are robust across assumptions for binary star evolution [42].

To disentangle hierarchical mergers from first-generation counterparts, it is useful to look in parameters that are both well-measured and in which we expect distinct behavior. The rapid spins, unequal mass ratios, and/or high masses of several individual events—namely, GW190521 [11], GW231123 [14] and GW241011 [43]—have led to their interpretation as hierarchical mergers [25, 44–47], though non-hierarchical interpretations have also been put forward [e.g. 24, 48–53]. However, data quality issues and waveform inaccuracies can introduce systematic biases in measurements of individual systems, including their spins [14, 54–57]. When per-

* caplunk@mit.edu

† www.sites.mit.edu/spins

forming and interpreting population analyses, we therefore turn to effective parameters, whose measurements may be more trustworthy than those of component spins and tilts [58–60]. Effective inspiral spin [61, 62] is typically the best-measured combination of spin parameters [63], defined as the mass-weighted projection of the spin vectors onto the orbital angular momentum: $\chi_{\text{eff}} = (a_1 \cos \tau_1 + q a_2 \cos \tau_2) / (1+q)$; where q denotes the mass ratio (defined on the range $0 < q \leq 1$), a_1 and a_2 are the respective spin magnitudes of the primary (heavier) and secondary (lighter) black holes, and $\tau_{1,2}$ are the angles between the spin vectors and the Newtonian orbital angular momentum at a chosen reference frequency. The natal spins of black holes are theoretically uncertain but often expected to be small [64–68], in which case mergers of two first-generation black holes (1G+1G) will have a narrow χ_{eff} distribution centered near zero. In contrast, hierarchical mergers between one first- and one second-generation black hole (1G+2G) will have a uniform χ_{eff} distribution centered at 0 with a width of ~ 1 . While higher-generation mergers (e.g., 1G+3G, 2G+2G) are possible, their rates are likely an order of magnitude below that of 1G+2G mergers [31, 69–71]; as such, we specialize to the distribution of 1G+2G mergers.

As spin parameters are useful differentiators between formation channels (including hierarchical assembly), many studies have searched for population-level signatures in χ_{eff} , spin magnitudes, and/or spin orientations, often in conjunction with mass dependence [72–92]. Recently, Refs. [86, 87] found indication of a population transition to higher spin magnitudes above $m_1 \sim 40\text{--}50 M_{\odot}$, and Refs. [88–92] presented strong evidence for a transition in χ_{eff} from a narrow Gaussian to primarily uniform above $m_1 \sim 45 M_{\odot}$. Refs. [90, 92] furthermore demonstrated the χ_{eff} transition to be coincident with a truncation in the secondary mass distribution, remarkably in line with the theoretical expectation for the lower edge of the PISN gap. These studies suggest that above $\sim 45 M_{\odot}$ the population is dominated by second-generation black holes.

Although effective spin has been a successful population-level diagnostic of hierarchical mergers, it is a lossy compression of the full six-dimensional spin space to a single parameter. Hierarchical mergers are distinguished from first-generation mergers not only in χ_{eff} , but cleanly in the *joint* space of χ_{eff} and effective precessing spin χ_p , which is a linearization of the in-plane spin dynamics [93, 94]: $\chi_p = \max[a_1 \sin \tau_1, (3+4q)/(4+3q) q a_2 \sin \tau_2]$. The joint $\chi_{\text{eff}}\text{--}\chi_p$ distribution for 1G+1G mergers is expected to cluster tightly near $\chi_{\text{eff}}, \chi_p \sim 0$. That of 1G+2G mergers, in comparison, scatters around the boundary of an ellipse centered on $\chi_{\text{eff}}, \chi_p = 0$ with major axis $\chi_p \approx 0.7$ and minor axis $\chi_{\text{eff}} \approx 0.47$ [88, 95]. Modeling in multiple dimensions can illuminate correlations and offer complementary confirmation of features identified with one-dimensional models.

In this Letter, we introduce an astrophysically-motivated population model in the joint space of effective inspiral and precessing spin. We include a two-dimensional ellipse-boundary component to capture 1G+2G mergers alongside a Gaussian to describe 1G+1G binaries. We explore the mixing fraction between these components as a function of mass and recover strong evidence for a subpopulation of hierarchical mergers at $\sim 15 M_{\odot}$ and a transition at $\sim 45 M_{\odot}$ beyond which the majority of mergers are hierarchical. Our results not only are consistent with studies that model only in χ_{eff} , but also reveal correlated structure in the χ_p distribution that increases credence both for the robustness of these features and their association with hierarchical mergers.

Models — We analyze BBHs in the Fourth Gravitational-Wave Transient Catalog (GWTC-4) [4] with false-alarm rates $< 1 \text{ yr}^{-1}$ alongside GW241011 and GW241110, two events from the second part of the fourth observing run whose spin properties hint at a hierarchical origin [43]. We model the population-level $\chi_{\text{eff}}\text{--}\chi_p$ distribution as a mixture of two components: a truncated Gaussian for the 1G+1G distribution and a probability density concentrated on an ellipse boundary for the 1G+2G distribution.¹

When secondary spin is negligible, $\chi_{\text{eff}} \approx a_1/(1+q) \cos \tau_1$ and $\chi_p \approx a_1 \sin \tau_1$. Second-generation black holes cluster around a characteristic spin $\chi_c = 0.7$ and have typical mass ratios $q_c \sim 0.5$ with their secondary. Coupled with isotropic tilts, the astrophysical distribution of 1G+2G mergers in the $\chi_{\text{eff}}\text{--}\chi_p$ plane follows the boundary of an ellipse with major axis $\chi_p = \chi_c = 0.7$, minor axis $\chi_{\text{eff}} = \chi_c/(1+q_c) = 0.47$, uniform marginal χ_{eff} , and marginal χ_p declining by $p(\chi_p) \propto \chi_p / (\chi_c^2 - \chi_p^2)^{1/2}$ [88, 95]. The separation between first-generation and hierarchical mergers, and the latter's elliptical structure, is pictured in Fig. 1 of Ref. [96] with the $\chi_{\text{eff}}\text{--}\chi_p$ distribution for simulated dynamical mergers from the CLUSTER MONTE CARLO (CMC) catalog [69, 70].

We model the probability density for 1G+2G mergers as a Gaussian in the perpendicular distance from an ellipse boundary with a filter along χ_p to account for the declining density. The characteristic spin χ_c , characteristic mass ratio q_c , and Gaussian width $\ln \sigma$ are inferred from the data. Fig. 1 schematically depicts the components of this model.

We allow the mixing fraction between the Gaussian (1G+1G) and ellipse-boundary (1G+2G) components to vary with primary mass, similar to the models employed in Refs. [91, 92]. We use a cubic spline to flexibly model

¹ Throughout, we associate the Gaussian and elliptical components to 1G+1G and 1G+2G mergers, respectively, and refer to the model components with their associated astrophysical interpretations interchangeably.

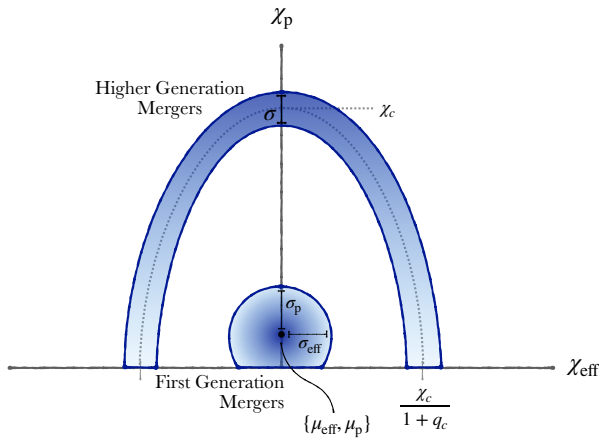


FIG. 1. Schematic of our two-component model in χ_{eff} – χ_p space. The truncated Gaussian describes 1G+1G mergers and is defined by its means $(\mu_{\text{eff},p})$ and standard deviations $(\sigma_{\text{eff},p})$ in both dimensions. The ellipse-boundary component, ascribed to 1G+2G mergers, is determined by a characteristic spin χ_c , characteristic mass ratio q_c , and Gaussian width perpendicular to the curve σ .

the branching ratio without imposing strong priors on the existence or location of transitions; the Supplemental Material contains specifics of our node choices.

For primary mass, we identically model both components with the GWTC-4 default, a broken power law with two Gaussian peaks and low-mass smoothing. While we use the standard power-law mass ratio model for the 1G+1G component, for the 1G+2G mergers we instead use a truncated normal, recognizing that hierarchical mergers may have a mass ratio peak away from unity. For both components, evolution over cosmic time is modeled with a power law. Mathematical details of all models are given in the Supplemental Material.

Results — In Fig. 2, we show the posterior distributions of χ_{eff} and χ_p for the ellipse-boundary (1G+2G) component. The main panel shows the median joint distribution while the marginals show the 90% credible regions of the posterior as well as of prior draws that pass the likelihood variance cut (see Supplemental Material). The characteristic spin value is inferred to be $\chi_c = 0.66^{+0.18}_{-0.28}$ ², in agreement with the expectation of $\chi_c = 0.7$ for 1G+2G mergers [39]. Fig. 2 illustrates the normalized density of the hierarchical component independent of its population fraction.

Fig. 3 plots the fraction of 1G+2G mergers, ξ , as a function of primary mass. Near $m_1 \sim 45 M_\odot$, the

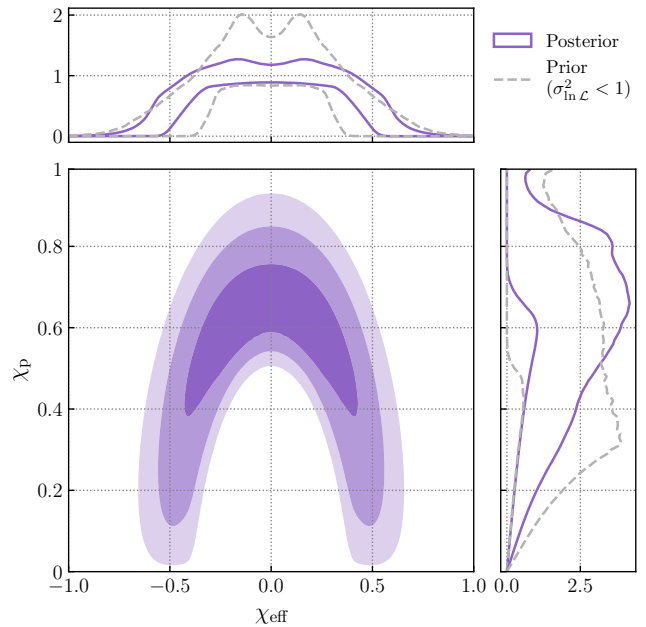


FIG. 2. Posterior on the ellipse-boundary component in χ_{eff} – χ_p space. The joint distribution plots the median inference, with 50%, 90%, and 99% percentile contours; side panels plot the 90% credible regions of the marginals, including those for prior draws that pass the likelihood variance threshold.

1G+2G fraction transitions from $\xi \approx 0$ to $\xi > 0$, consistent with Refs. [86–92]. Defining the transition point m_* by the horizontal slice of the posterior at $\xi = 0.5$ between $m_1 \in (30, 80) M_\odot$, we find $m_* = 46.3^{+21.9}_{-7.2} M_\odot$. The fraction of 1G+2G mergers is confidently constrained above zero above this transition—and is consistent with unity—until $\sim 100 M_\odot$. Beyond this mass, as well as below $\sim 7 M_\odot$, we roughly recover the prior on ξ due to the lack of data. Marginalized over primary mass, we find the total fraction of hierarchical mergers to be $\xi = 0.14^{+0.12}_{-0.07}$.

In addition to a high-mass population of hierarchical mergers, we observe evidence for a distinct subpopulation of 1G+2G mergers with masses $m_1 \in (13, 20) M_\odot$. The 1G+2G fraction is constrained to be $\gtrsim 5\%$ at the 99% level in this range. The existence of this low-mass population is compatible with the results of Refs. [91, 92], even as we expand the dimensionality of the problem by including precessing spin. Considering where each posterior sample achieves its maximum in this mass range, we find a peak in the fraction of hierarchical mergers at $m_{\text{peak}} = 15.7^{+3.2}_{-1.1} M_\odot$. Inference of this feature is not solely driven by the exceptional events GW241011 and GW241110, which lie in this mass regime and whose spin and tilt characteristics are consistent with 1G+2G; an analysis excluding these events recovers the lower peak albeit with greater uncertainty (see Supplemental Material). While the data suggest potentially a large fraction of mergers in 13 – $20 M_\odot$ are hierarchical, they also imply

² Here and elsewhere we quote the median and 90% symmetric credible interval.

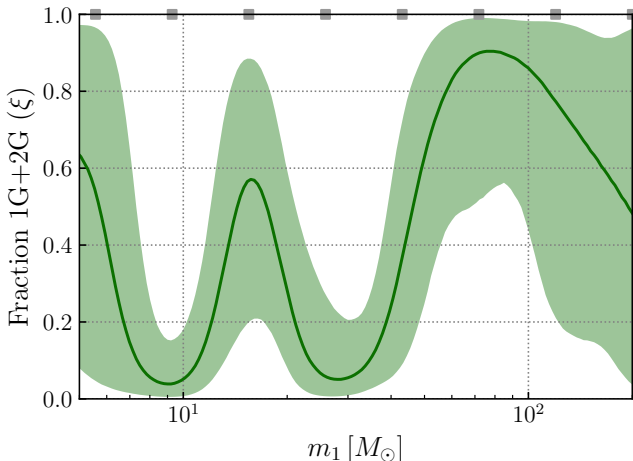


FIG. 3. The inferred fraction of hierarchical mergers $\xi(m_1)$. We plot the median and 90% symmetric credible interval. Gray squares mark the locations of the spline nodes.

few mergers in 20–40 M_\odot are: the $\chi_{\text{eff}}-\chi_p$ distribution is inferred to be primarily Gaussian for $m_1 \sim 8$ –10 M_\odot and $m_1 \sim 20$ –40 M_\odot . In fact, our tightest constraints on ξ are in these regimes where we infer a low proportion of hierarchical mergers. At $m_1 = 9 M_\odot$ ($30 M_\odot$), we constrain $\xi < 0.12$ ($\xi < 0.16$) at 90% credibility: the population at these masses is almost purely first-generation.

The astrophysically-informed ellipse-boundary $\chi_{\text{eff}}-\chi_p$ model for the hierarchical component induces, by design, a quasi-uniform marginal χ_{eff} akin to the one-dimensional model employed by Refs. [91, 92]. Hence, our comparable identification of spin-mass features is not unexpected. The addition of the χ_p dimension allows for richer inference of the population spin structure, such as the inferred spin magnitude peak at $\chi \approx 0.7$ for the ellipse component that further corroborates the hierarchical hypothesis. Further, we measure $\xi(m_1)$ with higher certainty than Ref. [92], which used only χ_{eff} . In particular, we constrain ξ away from unity near the low-mass peak and, importantly, more confidently infer a nonzero hierarchical fraction ($\xi > 0$) above the high-mass transition, finding a higher lower limit that extends across a broader mass regime: $\xi > 50\%$ for $m_1 \in [60, 100] M_\odot$ at 90% credibility.

The inclusion of the 1G+2G population significantly impacts the inferred spin distribution of the bulk BBH population. The width of the 1G+1G Gaussian is, foreseeably, narrower than when the hierarchical component is excluded. In χ_{eff} , the two-component model recovers $\sigma_{\chi_{\text{eff}}} = 0.07^{+0.02}_{-0.01}$, nearly half that of the Gaussian-only model, which returns $\sigma_{\chi_{\text{eff}}} = 0.13^{+0.03}_{-0.02}$. The mean of the χ_{eff} distribution remains constrained above zero, $\mu_{\chi_{\text{eff}}} = 0.03^{+0.01}_{-0.01}$. Neglecting the 1G+2G subpopulation will bias first-generation effective spin measurements by overestimating the population’s spread in χ_{eff} and χ_p .

The model including the hierarchical component, with the branching ratio an evolving function of mass, is preferred over a pure Gaussian model with a natural log Bayes factor of $\ln \mathcal{B} = 14.4$. It is favored over a model where the branching ratio is constant as a function of mass with $\ln \mathcal{B} = 6.8$. These Bayes factors indicate significant evidence for structure in the effective inspiral and precessing spin distribution consistent with hierarchical mergers, and, moreover, structure that is nonlinearly correlated with primary mass.

Discussion and conclusion — Using an astrophysically-informed mixture model in the joint $\chi_{\text{eff}}-\chi_p$ space, we find strong evidence for a subpopulation of binary black hole mergers that occupy the boundary of an ellipse with a characteristic spin near $\chi_c = 0.7$, consistent with the expectation for hierarchical mergers. Allowing the mixing fraction between the components to vary with primary mass, we identify a transition to primarily high spin and quasi-uniform χ_{eff} above $\sim 45 M_\odot$. Interpreting the ellipse component as hierarchical mergers, the data indicate most black holes above $45 M_\odot$ arise from repeated mergers in dense stellar clusters, aligned with the predicted onset of the pair-instability gap.

Moreover, we measure a peak in the fraction of hierarchical mergers between 14–16 M_\odot . Hierarchical assembly is frequently discussed as a method to produce black holes in and above the PISN gap, and, indeed, the transition near $45 M_\odot$ corroborates this interpretation. However, accounting for the expected evolution of cluster metallicity across cosmic time, simulations of dense stellar clusters suggest the second-generation mass spectrum declines with primary mass and peaks near $15 M_\odot$, driven by an abundance of low-mass first-generation black holes produced by solar-metallicity stars [31, 69, 71, 97]. As such, the existence of this lower peak is unsurprising and may constitute the maximum of the 2G mass spectrum. At the same time, second-generation black holes above $45 M_\odot$ are uncommon in near-solar-metallicity clusters, potentially implying the high-mass component arises from clusters with different initial conditions—namely, lower metallicities—than the low-mass population. Coupling the features in the data with predictions from stellar evolution may enable constraints on the metallicity distribution of the progenitor stars of black-hole mergers.

While the low-mass peak meshes with theoretical expectation, the ostensible *lack* of hierarchical mergers between 20 and 40 M_\odot is perhaps more surprising. The dominance of hierarchical mergers in the 10–20 M_\odot range followed by the dearth in 20–40 M_\odot may imply either a dip in the first-generation mass spectrum in the former range, or a pile-up in the latter. A drop in progenitor core compactness may drive a dip in this lower regime [98], for which several studies have searched and some have tentatively identified [99–101]. If the observed peak at

$\sim 35M_\odot$ is composed of primarily first-generation mergers, it may also contribute to the apparent lack of second-generation black holes at moderate masses. Untangling what the inferred branching fraction across primary mass indicates for both the first- and second-generation mass spectra—and the properties of their stellar progenitors—is a key avenue for future study.

We find reduced uncertainty in $\xi(m_1)$ compared to the χ_{eff} -only analysis of Ref. [92], particularly higher credence for a nonzero hierarchical fraction above $45M_\odot$. We ascribe the improved constraint to information in the χ_p dimension, although we cannot rule out that other details of the model may have contributed.

Taken at face value, the fraction of hierarchical mergers inferred from GW data is consistent with a population made of entirely dynamical mergers. We find the total 1G+2G fraction to be $\xi \sim 14\%$, while 1G+2G mergers comprise $\sim 17\%$ of all cluster mergers in the simulated CMC catalog [69, 70]. Incorporating the expected distribution of clusters, the astrophysical hierarchical fraction is likely closer to $\sim 10\%$ [97, 102]. The inferred first-generation spin distribution continues to have support at negative χ_{eff} , which may signify dynamical mergers; that said, its confidently positive centroid is indicative of isolated binaries. We caution against over-interpreting the similarity between the inferred hierarchical proportion and that from simulations, as the former relies on associating the ellipse-boundary component to 1G+2G mergers and the latter on theoretically uncertain physical prescriptions that control the merger rate, such as the escape velocity distribution.

Sequential mergers may also occur in AGN disks or triple systems [25, 26, 103–106]. These mechanisms likely produce preferentially aligned mergers, as opposed to the isotropic tilts found in clusters. An asymmetric ellipse component is slightly disfavored (see Supplemental Material), suggesting AGN- or triple-driven mergers are not dominant constituents of the observed ellipse-like $\chi_{\text{eff}}-\chi_p$ distribution. Further observations may allow us to elucidate hierarchical subpopulations corresponding to different mechanisms that prompt the repeated mergers.

Linking the black-hole mass spectrum to features in the spin distribution is a promising avenue to more precisely identify hallmarks of stellar evolution that may otherwise be washed out, like the pair-instability mass gap, by combining information across multiple dimensions. Improved constraints on the pair-instability gap will sharpen bounds on nuclear processes inaccessible at laboratory temperatures, in particular the cross-section of the $^{12}\text{C}(\alpha, \gamma)^{16}\text{O}$ reaction, pivotal to energy production in massive stars [22, 107, 108]. As the catalog of binary black hole mergers continues to grow alongside advancements in stellar theory and simulation, the statistical significance and associated astrophysical interpretation of spin-mass features in the population will be tested with increasing rigor, emphasizing the power of

astrophysically-informed population studies to uncover the evolutionary history of black holes.

Acknowledgments — We thank Fabio Antonini, Sharan Banagiri, Thomas Dent, Maya Fishbach, Asad Hussain, Matthew Mould, Gregoire Pierra, Vaibhav Tiwari, and Hui Tong for discussions. C.P. is supported by the National Science Foundation Graduate Research Fellowship under Grant No. DGE-2141064. M.Z. gratefully acknowledges funding from the Brinson Foundation in support of astrophysics research at the Adler Planetarium. S.V. is partially supported by the NSF grant No. PHY-2045740.

The authors are grateful for computational resources provided by the LIGO Laboratory supported by National Science Foundation Grants PHY-0757058 and PHY-0823459. This material is based upon work supported by NSF’s LIGO Laboratory which is a major facility fully funded by the National Science Foundation and has made use of data or software obtained from the Gravitational Wave Open Science Center (gwosc.org), a service of the LIGO Scientific Collaboration, the Virgo Collaboration, and KAGRA.

Data availability —The data that support the findings of this article will be made openly available at Ref. [109] upon publication.

- [1] I. Mandel and A. Farmer, *Phys. Rept.* **955**, 1 (2022), [arXiv:1806.05820 \[astro-ph.HE\]](https://arxiv.org/abs/1806.05820).
- [2] M. Mapelli, Formation Channels of Single and Binary Stellar-Mass Black Holes (2021) [arXiv:2106.00699 \[astro-ph.HE\]](https://arxiv.org/abs/2106.00699).
- [3] I. Mandel and F. S. Broekgaarden, *Living Rev. Rel.* **25**, 1 (2022), [arXiv:2107.14239 \[astro-ph.HE\]](https://arxiv.org/abs/2107.14239).
- [4] A. G. Abac *et al.* (LIGO Scientific, VIRGO, KAGRA), (2025), [arXiv:2508.18082 \[gr-qc\]](https://arxiv.org/abs/2508.18082).
- [5] A. G. Abac *et al.* (LIGO Scientific, VIRGO, KAGRA), (2025), [arXiv:2508.18083 \[astro-ph.HE\]](https://arxiv.org/abs/2508.18083).
- [6] J. Aasi *et al.* (LIGO Scientific), *Class. Quant. Grav.* **32**, 074001 (2015), [arXiv:1411.4547 \[gr-qc\]](https://arxiv.org/abs/1411.4547).
- [7] E. Capote *et al.*, *Phys. Rev. D* **111**, 062002 (2025), [arXiv:2411.14607 \[gr-qc\]](https://arxiv.org/abs/2411.14607).
- [8] S. Soni *et al.* (LIGO), *Class. Quant. Grav.* **42**, 085016 (2025), [arXiv:2409.02831 \[astro-ph.IM\]](https://arxiv.org/abs/2409.02831).
- [9] F. Acernese *et al.* (VIRGO), *Class. Quant. Grav.* **32**, 024001 (2015), [arXiv:1408.3978 \[gr-qc\]](https://arxiv.org/abs/1408.3978).
- [10] T. Akutsu *et al.* (KAGRA), *PTEP* **2021**, 05A101 (2021), [arXiv:2005.05574 \[physics.ins-det\]](https://arxiv.org/abs/2005.05574).
- [11] R. Abbott *et al.* (LIGO Scientific, Virgo), *Phys. Rev. Lett.* **125**, 101102 (2020), [arXiv:2009.01075 \[gr-qc\]](https://arxiv.org/abs/2009.01075).
- [12] R. Abbott *et al.* (KAGRA, VIRGO, LIGO Scientific), *Phys. Rev. X* **13**, 011048 (2023), [arXiv:2111.03634 \[astro-ph.HE\]](https://arxiv.org/abs/2111.03634).
- [13] B. Edelman, Z. Doctor, and B. Farr, *Astrophys. J. Lett.* **913**, L23 (2021), [arXiv:2104.07783 \[astro-ph.HE\]](https://arxiv.org/abs/2104.07783).
- [14] A. G. Abac *et al.* (LIGO Scientific, VIRGO, KAGRA), *Astrophys. J. Lett.* **993**, L25 (2025), [arXiv:2507.08219](https://arxiv.org/abs/2507.08219)

[astro-ph.HE].

[15] W. A. Fowler and F. Hoyle, *Astrophys. J. Suppl.* **9**, 201 (1964).

[16] Z. Barkat, G. Rakavy, and N. Sack, *Phys. Rev. Lett.* **18**, 379 (1967).

[17] G. Rakavy and G. Shaviv, *Astrophys. J.* **148**, 803 (1967).

[18] G. S. Fraley, *Astrophysics and Space Science* **2**, 96 (1968).

[19] A. Heger, C. L. Fryer, S. E. Woosley, N. Langer, and D. H. Hartmann, *Astrophys. J.* **591**, 288 (2003), arXiv:astro-ph/0212469.

[20] R. Farmer, M. Renzo, S. E. de Mink, P. Marchant, and S. Justham 10.3847/1538-4357/ab518b (2019), arXiv:1910.12874 [astro-ph.SR].

[21] S. Stevenson, M. Sampson, J. Powell, A. Vigna-Gómez, C. J. Neijssel, D. Szécsi, and I. Mandel 10.3847/1538-4357/ab3981 (2019), arXiv:1904.02821 [astro-ph.HE].

[22] R. Farmer, M. Renzo, S. de Mink, M. Fishbach, and S. Justham, *Astrophys. J. Lett.* **902**, L36 (2020), arXiv:2006.06678 [astro-ph.HE].

[23] S. E. Woosley and A. Heger, *Astrophys. J. Lett.* **912**, L31 (2021), arXiv:2103.07933 [astro-ph.SR].

[24] E. J. Farrell, J. H. Groh, R. Hirschi, L. Murphy, E. Kaiser, S. Ekström, C. Georgy, and G. Meynet, *Mon. Not. Roy. Astron. Soc.* **502**, L40 (2021), arXiv:2009.06585 [astro-ph.SR].

[25] H. Tagawa, B. Kocsis, Z. Haiman, I. Bartos, K. Omukai, and J. Samsing, *Astrophys. J.* **908**, 194 (2021), arXiv:2012.00011 [astro-ph.HE].

[26] M. P. Vaccaro, M. Mapelli, C. Périgois, D. Barone, M. C. Artale, M. Dall’Amico, G. Iorio, and S. Torniamenti, *Astron. Astrophys.* **685**, A51 (2024), arXiv:2311.18548 [astro-ph.HE].

[27] E. R. J. Winch, J. S. Vink, E. R. Higgins, and G. N. Sabahatif, *Mon. Not. Roy. Astron. Soc.* **529**, 2980 (2024), arXiv:2401.17327 [astro-ph.HE].

[28] S. Torniamenti, M. Mapelli, C. Périgois, M. A. Sedda, M. C. Artale, M. Dall’Amico, and M. P. Vaccaro, *Astron. Astrophys.* **688**, A148 (2024), arXiv:2401.14837 [astro-ph.HE].

[29] R. M. O’Leary, F. A. Rasio, J. M. Fregeau, N. Ivanova, and R. W. O’Shaughnessy, *Astrophys. J.* **637**, 937 (2006), arXiv:astro-ph/0508224.

[30] F. Antonini and F. A. Rasio, *Astrophys. J.* **831**, 187 (2016), arXiv:1606.04889 [astro-ph.HE].

[31] C. L. Rodriguez, M. Zevin, P. Amaro-Seoane, S. Chatterjee, K. Kremer, F. A. Rasio, and C. S. Ye, *Phys. Rev. D* **100**, 043027 (2019), arXiv:1906.10260 [astro-ph.HE].

[32] Z. Doctor, D. Wysocki, R. O’Shaughnessy, D. E. Holz, and B. Farr 10.3847/1538-4357/ab7fac (2019), arXiv:1911.04424 [astro-ph.HE].

[33] P. Mahapatra, D. Chattopadhyay, A. Gupta, F. Antonini, M. Favata, B. S. Sathyaprakash, and K. G. Arun, *Astrophys. J.* **975**, 117 (2024), arXiv:2406.06390 [astro-ph.HE].

[34] M. A. Sedda, A. W. H. Kamlah, R. Spurzem, F. P. Rizzato, M. Giersz, T. Naab, and P. Berczik, *Mon. Not. Roy. Astron. Soc.* **528**, 5140 (2024), arXiv:2307.04807 [astro-ph.HE].

[35] F. Pretorius, *Phys. Rev. Lett.* **95**, 121101 (2005), arXiv:gr-qc/0507014.

[36] A. Buonanno, L. E. Kidder, and L. Lehner, *Phys. Rev. D* **77**, 026004 (2008), arXiv:0709.3839 [astro-ph].

[37] W. Tichy and P. Marronetti, *Phys. Rev. D* **78**, 081501 (2008), arXiv:0807.2985 [gr-qc].

[38] L. Rezzolla, E. Barausse, E. N. Dorband, D. Pollney, C. Reisswig, J. Seiler, and S. Husa, *Phys. Rev. D* **78**, 044002 (2008), arXiv:0712.3541 [gr-qc].

[39] F. Hofmann, E. Barausse, and L. Rezzolla, *Astrophys. J. Lett.* **825**, L19 (2016), arXiv:1605.01938 [gr-qc].

[40] M. Zevin and D. E. Holz, *Astrophys. J. Lett.* **935**, L20 (2022), arXiv:2205.08549 [astro-ph.HE].

[41] A. Borchers, C. S. Ye, and M. Fishbach, *Astrophys. J.* **987**, 10.3847/1538-4357/addec6 (2025), arXiv:2503.21278 [astro-ph.HE].

[42] M. Fishbach, D. E. Holz, and B. Farr, *Astrophys. J. Lett.* **840**, L24 (2017), arXiv:1703.06869 [astro-ph.HE].

[43] A. G. Abac *et al.* (LIGO Scientific, Virgo, KAGRA), *Astrophys. J. Lett.* **993**, L21 (2025), arXiv:2510.26931 [astro-ph.HE].

[44] R. Abbott *et al.* (LIGO Scientific, Virgo), *Astrophys. J. Lett.* **900**, L13 (2020), arXiv:2009.01190 [astro-ph.HE].

[45] C. Kimball *et al.*, *Astrophys. J. Lett.* **915**, L35 (2021), arXiv:2011.05332 [astro-ph.HE].

[46] V. Gayathri, Y. Yang, H. Tagawa, Z. Haiman, and I. Bartos, *Astrophys. J. Lett.* **920**, L42 (2021), arXiv:2104.10253 [gr-qc].

[47] D. Gerosa and M. Fishbach, *Nature Astron.* **5**, 749 (2021), arXiv:2105.03439 [astro-ph.HE].

[48] M. Fishbach and D. E. Holz, *Astrophys. J. Lett.* **904**, L26 (2020), arXiv:2009.05472 [astro-ph.HE].

[49] T. Kinugawa, T. Nakamura, and H. Nakano, *Mon. Not. Roy. Astron. Soc.* **501**, L49 (2021), arXiv:2009.06922 [astro-ph.HE].

[50] S. A. Popa and S. E. de Mink, (2025), arXiv:2509.00154 [astro-ph.HE].

[51] O. Gottlieb, B. D. Metzger, D. Issa, S. E. Li, M. Renzo, and M. Isi, *Astrophys. J. Lett.* **993**, L54 (2025), arXiv:2508.15887 [astro-ph.HE].

[52] D. Croon, J. Sakstein, and D. Gerosa, (2025), arXiv:2508.10088 [astro-ph.HE].

[53] I. Bartos and Z. Haiman, (2025), arXiv:2508.08558 [astro-ph.HE].

[54] R. Abbott *et al.* (KAGRA, VIRGO, LIGO Scientific), *Phys. Rev. X* **13**, 041039 (2023), arXiv:2111.03606 [gr-qc].

[55] E. Payne, S. HouriHane, J. Golomb, R. Udall, R. Udall, D. Davis, and K. Chatzioannou, *Phys. Rev. D* **106**, 104017 (2022), arXiv:2206.11932 [gr-qc].

[56] R. Udall, S. Bini, K. Chatzioannou, D. Davis, S. HouriHane, Y. Lecoeuche, J. McIver, and S. Miller, (2025), arXiv:2510.05029 [gr-qc].

[57] A. Ray, S. Banagiri, E. Thrane, and P. D. Lasky, (2025), arXiv:2510.07228 [gr-qc].

[58] R. Macas, A. Lundgren, and G. Ashton, *Phys. Rev. D* **109**, 062006 (2024), arXiv:2311.09921 [gr-qc].

[59] S. J. Miller, Z. Ko, T. Callister, and K. Chatzioannou, *Phys. Rev. D* **109**, 104036 (2024), arXiv:2401.05613 [gr-qc].

[60] S. Vitale, S. Biscoveanu, and C. Talbot, *Astron. Astrophys.* **668**, L2 (2022), arXiv:2209.06978 [astro-ph.HE].

[61] E. Racine, *Phys. Rev. D* **78**, 044021 (2008), arXiv:0803.1820 [gr-qc].

[62] D. Gerosa and E. Berti, *Phys. Rev. D* **95**, 124046 (2017), arXiv:1703.06223 [gr-qc].

[63] S. Vitale, R. Lynch, V. Raymond, R. Sturani, J. Veitch, and P. Graff, *Phys. Rev. D* **95**, 064053 (2017),

arXiv:1611.01122 [gr-qc].

[64] H. C. Spruit, *Astron. Astrophys.* **381**, 923 (2002), arXiv:astro-ph/0108207.

[65] Y. Qin, T. Fragos, G. Meynet, J. Andrews, M. Sørensen, and H. F. Song, *Astron. Astrophys.* **616**, A28 (2018), arXiv:1802.05738 [astro-ph.SR].

[66] J. Fuller and L. Ma, *Astrophys. J. Lett.* **881**, L1 (2019), arXiv:1907.03714 [astro-ph.SR].

[67] J. Fuller and W. Lu, *Mon. Not. Roy. Astron. Soc.* **511**, 3951 (2022), arXiv:2201.08407 [astro-ph.HE].

[68] A. Burrows, T. Wang, D. Vartanyan, and M. S. B. Coleman, *Astrophys. J.* **963**, 63 (2024), arXiv:2311.12109 [astro-ph.HE].

[69] K. Kremer, C. S. Ye, N. Z. Rui, N. C. Weatherford, S. Chatterjee, G. Fragione, C. L. Rodriguez, M. Spera, and F. A. Rasio, *Astrophys. J. Suppl.* **247**, 48 (2020), arXiv:1911.00018 [astro-ph.HE].

[70] C. L. Rodriguez *et al.*, *Astrophys. J. Suppl.* **258**, 22 (2022), arXiv:2106.02643 [astro-ph.GA].

[71] C. S. Ye and M. Fishbach, *Astrophys. J.* **967**, 62 (2024), arXiv:2402.12444 [astro-ph.HE].

[72] S. Stevenson, C. P. L. Berry, and I. Mandel, *Mon. Not. Roy. Astron. Soc.* **471**, 2801 (2017), arXiv:1703.06873 [astro-ph.HE].

[73] M. Safarzadeh, W. M. Farr, and E. Ramirez-Ruiz, *Astrophys. J.* **894**, 129 (2020), arXiv:2001.06490 [gr-qc].

[74] V. Tiwari and S. Fairhurst, *Astrophys. J. Lett.* **913**, L19 (2021), arXiv:2011.04502 [astro-ph.HE].

[75] C. Hoy, S. Fairhurst, M. Hannam, and V. Tiwari, *Astrophys. J.* **928**, 75 (2022), arXiv:2110.13542 [gr-qc].

[76] H. Tagawa, Z. Haiman, I. Bartos, B. Kocsis, and K. Omukai, *Mon. Not. Roy. Astron. Soc.* **507**, 3362 (2021), arXiv:2104.09510 [astro-ph.HE].

[77] M. Mould, D. Gerosa, and S. R. Taylor, *Phys. Rev. D* **106**, 103013 (2022), arXiv:2203.03651 [astro-ph.HE].

[78] M. Fishbach, C. Kimball, and V. Kalogera, *Astrophys. J. Lett.* **935**, L26 (2022), arXiv:2207.02924 [astro-ph.HE].

[79] Y.-Z. Wang, Y.-J. Li, J. S. Vink, Y.-Z. Fan, S.-P. Tang, Y. Qin, and D.-M. Wei, *Astrophys. J. Lett.* **941**, L39 (2022), arXiv:2208.11871 [astro-ph.HE].

[80] Y.-J. Li, Y.-Z. Wang, S.-P. Tang, and Y.-Z. Fan, *Phys. Rev. Lett.* **133**, 051401 (2024), arXiv:2303.02973 [astro-ph.HE].

[81] A. Hussain, M. Isi, and A. Zimmerman, (2024), arXiv:2411.02252 [astro-ph.HE].

[82] A. Ray, I. Magaña Hernandez, K. Breivik, and J. Creighton, *Astrophys. J.* **991**, 17 (2025), arXiv:2404.03166 [astro-ph.HE].

[83] C. Adamcewicz, N. Guttman, P. D. Lasky, and E. Thrane, *Astrophys. J.* **994**, 261 (2025), arXiv:2509.04706 [astro-ph.HE].

[84] V. Tiwari, (2025), arXiv:2510.25579 [astro-ph.HE].

[85] E. Berti, F. Cressimbeni, G. Franciolini, S. Mastrogiovanni, P. Pani, and G. Pierra, (2025), arXiv:2512.03152 [gr-qc].

[86] G. Pierra, S. Mastrogiovanni, and S. Perriès, *Astron. Astrophys.* **692**, A80 (2024), arXiv:2406.01679 [gr-qc].

[87] S. Banagiri, E. Thrane, and P. D. Lasky, (2025), arXiv:2509.15646 [astro-ph.HE].

[88] F. Antonini, I. M. Romero-Shaw, and T. Callister, *Phys. Rev. Lett.* **134**, 011401 (2025), arXiv:2406.19044 [astro-ph.HE].

[89] F. Antonini, T. Callister, F. Dosopoulou, I. M. Romero-Shaw, and D. Chattopadhyay, *Phys. Rev. D* **112**, 063040 (2025), arXiv:2506.09154 [astro-ph.HE].

[90] H. Tong *et al.*, (2025), arXiv:2509.04151 [astro-ph.HE].

[91] F. Antonini, I. Romero-Shaw, T. Callister, F. Dosopoulou, D. Chattopadhyay, M. Gieles, and M. Mapelli, (2025), arXiv:2509.04637 [astro-ph.HE].

[92] H. Tong, T. A. Callister, M. Fishbach, E. Thrane, F. Antonini, S. Stevenson, I. M. Romero-Shaw, and F. Dosopoulou, (2025), arXiv:2511.05316 [astro-ph.HE].

[93] P. Schmidt, F. Ohme, and M. Hannam, *Phys. Rev. D* **91**, 024043 (2015), arXiv:1408.1810 [gr-qc].

[94] D. Gerosa, M. Mould, D. Gangardt, P. Schmidt, G. Pratten, and L. M. Thomas, *Phys. Rev. D* **103**, 064067 (2021), arXiv:2011.11948 [gr-qc].

[95] V. Baibhav, D. Gerosa, E. Berti, K. W. K. Wong, T. Helfer, and M. Mould, *Phys. Rev. D* **102**, 043002 (2020), arXiv:2004.00650 [astro-ph.HE].

[96] E. Payne, K. Kremer, and M. Zevin, *Astrophys. J. Lett.* **966**, L16 (2024), arXiv:2402.15066 [gr-qc].

[97] C. S. Ye, M. Fishbach, K. Kremer, and M. Reina-Campos, (2025), arXiv:2507.07183 [astro-ph.HE].

[98] F. R. N. Schneider, P. Podsiadlowski, and B. Müller, *Astron. Astrophys.* **645**, A5 (2021), arXiv:2008.08599 [astro-ph.SR].

[99] S. Galaudage and A. Lamberts, *Astron. Astrophys.* **694**, A186 (2025), arXiv:2407.17561 [astro-ph.HE].

[100] C. Adamcewicz, P. D. Lasky, E. Thrane, and I. Mandel, *Astrophys. J.* **975**, 253 (2024), arXiv:2406.11111 [astro-ph.HE].

[101] R. Willcox, F. R. N. Schneider, E. Laplace, P. Podsiadlowski, K. Maltsev, I. Mandel, P. Marchant, H. Sana, T. G. F. Li, and T. Hertog, (2025), arXiv:2510.07573 [astro-ph.SR].

[102] C. Plunkett *et al.* (2026), in preparation.

[103] Y. Yang *et al.*, *Phys. Rev. Lett.* **123**, 181101 (2019), arXiv:1906.09281 [astro-ph.HE].

[104] A. Vigna-Gómez, S. Toonen, E. Ramirez-Ruiz, N. W. C. Leigh, J. Riley, and C.-J. Haster, *Astrophys. J. Lett.* **907**, L19 (2021), arXiv:2010.13669 [astro-ph.HE].

[105] A. Dorozsmai, I. M. Romero-Shaw, A. Vijaykumar, S. Toonen, F. Antonini, K. Kremer, M. Zevin, and E. Grishin, (2025), arXiv:2507.23212 [astro-ph.GA].

[106] Y.-J. Li, Y.-Z. Wang, S.-P. Tang, and Y.-Z. Fan, (2025), arXiv:2509.23897 [astro-ph.HE].

[107] R. J. deBoer *et al.*, *Rev. Mod. Phys.* **89**, 035007 (2017), arXiv:1709.03144 [nucl-ex].

[108] G. Costa, A. Bressan, M. Mapelli, P. Marigo, G. Iorio, and M. Spera, *Mon. Not. Roy. Astron. Soc.* **501**, 4514 (2021), arXiv:2010.02242 [astro-ph.SR].

[109] C. Plunkett, T. Callister, M. Zevin, and S. Vitale, The data supporting the results of this study will be made available upon publication. (2025).

[110] J. S. Speagle, *Mon. Not. Roy. Astron. Soc.* **493**, 3132 (2020), arXiv:1904.02180 [astro-ph.IM].

[111] G. Ashton *et al.*, *Astrophys. J. Suppl.* **241**, 27 (2019), arXiv:1811.02042 [astro-ph.IM].

[112] I. Mandel, W. M. Farr, and J. R. Gair, *Mon. Not. Roy. Astron. Soc.* **486**, 1086 (2019), arXiv:1809.02063 [physics.data-an].

[113] S. Vitale, D. Gerosa, W. M. Farr, and S. R. Taylor 10.1007/978-981-15-4702-7_45-1 (2020), arXiv:2007.05579 [astro-ph.IM].

- [114] C. Talbot, A. Farah, S. Galauadage, J. Golomb, and H. Tong, *J. Open Source Softw.* **10**, 7753 (2025), [arXiv:2409.14143 \[astro-ph.IM\]](https://arxiv.org/abs/2409.14143).
- [115] LIGO Scientific Collaboration, Virgo Collaboration, and KAGRA Collaboration, *GWTC-4.0: Parameter estimation data release* (2025).
- [116] LIGO Scientific Collaboration, Virgo Collaboration, and KAGRA Collaboration, *GW241011 and GW241110: Exploring binary formation and fundamental physics with asymmetric, high-spin black hole coalescences* (2025).
- [117] G. Pratten *et al.*, *Phys. Rev. D* **103**, 104056 (2021), [arXiv:2004.06503 \[gr-qc\]](https://arxiv.org/abs/2004.06503).
- [118] R. Essick *et al.*, *Phys. Rev. D* **112**, 102001 (2025), [arXiv:2508.10638 \[gr-qc\]](https://arxiv.org/abs/2508.10638).
- [119] R. Essick and W. Farr, (2022), [arXiv:2204.00461 \[astro-ph.IM\]](https://arxiv.org/abs/2204.00461).
- [120] J. Heinzel and S. Vitale, (2025), [arXiv:2509.07221 \[astro-ph.HE\]](https://arxiv.org/abs/2509.07221).
- [121] S. Banagiri, T. A. Callister, C. Adamcewicz, Z. Doctor, and V. Kalogera, *Astrophys. J.* **990**, 147 (2025), [arXiv:2501.06712 \[astro-ph.HE\]](https://arxiv.org/abs/2501.06712).

SUPPLEMENTAL MATERIAL

Model details

The relation between χ_{eff} and χ_p when secondary spin is small is well-described by

$$\chi_p^2 = a_1^2 - (1+q)^2 \chi_{\text{eff}}^2. \quad (1)$$

We can model this distribution with a curve defining an ellipse

$$F(\chi_{\text{eff}}, \chi_p | \chi_c, q_c) = \left(\frac{1+q_c}{\chi_c} \right)^2 \chi_{\text{eff}}^2 + \frac{1}{\chi_c^2} \chi_p^2 - 1 = 0, \quad (2)$$

where χ_c and q_c are the characteristic primary spin and mass ratio. We model the probability density for this component as a Gaussian in the distance to the curve. To linear order, the perpendicular distance from a point $(\chi_{\text{eff}}, \chi_p)$ to F is

$$d(\chi_{\text{eff}}, \chi_p | \chi_c, q_c) \approx \frac{|F(\chi_{\text{eff}}, \chi_p | \chi_c, q_c)|}{\|\nabla F(\chi_{\text{eff}}, \chi_p | \chi_c, q_c)\|} \quad (3)$$

$$= \frac{\left| \frac{\chi_{\text{eff}}^2}{(\chi_c/(1+q_c))^2} + \frac{\chi_p^2}{\chi_c^2} - 1 \right|}{2 \left(\frac{\chi_{\text{eff}}^2}{(\chi_c/(1+q_c))^4} + \frac{\chi_p^2}{\chi_c^4} \right)^{1/2}}. \quad (4)$$

The density at $(\chi_{\text{eff}}, \chi_p)$ is thus

$$\mathcal{N}(\chi_{\text{eff}}, \chi_p | \chi_c, q_c, \sigma) \propto \exp \left(-\frac{d(\chi_{\text{eff}}, \chi_p | \chi_c, q_c)^2}{2\sigma^2} \right). \quad (5)$$

An isotropic tilt angle distribution, as expected for hierarchical mergers, corresponds to a $\sin \tau_1$ distribution

diverging at unity, $p(\sin \tau_1) \propto \sin \tau_1 / \sqrt{1 - \sin^2 \tau_1}$. The marginal distribution of χ_p thus peaks at χ_c following

$$p(\chi_p) \propto \begin{cases} \frac{\chi_p}{\sqrt{\chi_c^2 - \chi_p^2}}, & \chi_p < \chi_c; \\ 0, & \chi_p \geq \chi_c. \end{cases} \quad (6)$$

As divergent behavior and sharp cutoffs are problematic to model, we instead accommodate this falloff with the filter $f(\chi_p) = \chi_p / \sqrt{1 - \chi_p^2}$. While this approximation lacks steepness toward χ_c , we find the Gaussian overlay accommodates the necessary density toward χ_c such that this model can reproduce the marginal χ_p distribution of simulated 1G+2G mergers [31, 69] quite accurately. The total probability density for the ellipse component is

$$p_{1\text{G}+2\text{G}}(\chi_{\text{eff}}, \chi_p | \chi_c, q_c, \sigma) = \mathcal{N}(\chi_{\text{eff}}, \chi_p | \chi_c, q_c, \sigma) f(\chi_p). \quad (7)$$

The width parameter σ captures the expected spread in the $\chi_{\text{eff}} - \chi_p$ distribution due to the varying mass ratios and precise spin values of 2G mergers. We fit for the width and characteristic spin and mass ratio values with priors listed in Tab. I.

Hierarchical Bayesian inference

We sample the population posterior using *Dynesty* [110] and *Bilby* [111] with the population likelihood [112, 113] as implemented in *GWPopulation* [114]. Our catalog consists of the 153 binary black holes in GWTC-4 [4] and the special events GW241011 and GW241110 [43]. We use the MIXED waveform results in the publicly-released posterior samples [115, 116] for most events, but reduce the parameter estimation contribution to the log-likelihood variance by instead using the IMRPHENOMXPHM [117] results for GW150914 and GW200129, which have fewer than 5000 MIXED samples. We estimate survey sensitivity with the public set of BBH injections recovered by search pipelines spanning all four observing runs [118].

We limit the log-likelihood variance from the Monte Carlo approximations in the likelihood to be smaller than 1, a condition shown to be sufficient to prevent bias in the posterior [119, 120]. We compute the error statistic introduced in Ref. [120] and find an information loss of 0.18 bits, within the suggested threshold. To test the impact of the variance cut, we also run with a limit of 4. The primary difference is in the inferred 1G+1G χ_p distribution, which is narrower and closer to zero than found with a variance cut of 1. While the data seemingly prefer small χ_p values, our inferential capability is limited in that regime predominantly due to selection variance.

For the primary mass model, we adopt the standard priors used by the LVK [5]. To improve prior draw efficiency, we limit the prior on the redshift power-law index to $\mathcal{U}(0, 10)$ as the entire posterior is contained above zero.

Symbol	Description	Prior
ξ	Fraction of 1G+2G black holes	$\mathcal{U}(0, 1)$
f_i	i^{th} spline node latent value	$\mathcal{N}(0, 2)$
λ	redshift power-law index	$\mathcal{U}(0, 10)$
α_1	m_1 power-law index below break	$\mathcal{U}(-4, 12)$
α_2	m_1 power-law index above break	$\mathcal{U}(-4, 12)$
b_m	m_1 power-law break mass	$\mathcal{U}(20, 50)$
μ_1	Lower m_1 peak mean [M_\odot]	$\mathcal{U}(5, 20)$
μ_2	Higher m_1 peak mean [M_\odot]	$\mathcal{U}(25, 60)$
σ_1	Lower m_1 peak width [M_\odot]	$\mathcal{U}(0, 10)$
σ_2	Higher m_1 peak width [M_\odot]	$\mathcal{U}(0, 10)$
λ_0	m_1 power law fraction	Dirichlet
λ_1	m_1 lower peak fraction	Dirichlet
λ_2	m_1 higher peak fraction	Dirichlet
$\delta_{\min,1}$	m_1 low-mass smoothing width [M_\odot]	$\mathcal{U}(0, 10)$
$\delta_{\min,2}$	m_2 low-mass smoothing width [M_\odot]	$\mathcal{U}(0, 10)$
$m_{\min,1}$	m_1 minimum mass [M_\odot]	$\mathcal{U}(3, 10)$
$m_{\min,2}$	m_2 minimum mass [M_\odot]	$\mathcal{U}(3, 10)$
m_{\max}	Maximum mass [M_\odot]	= 200
β	1G+1G q power-law index	$\mathcal{U}(-2, 7)$
μ_q	1G+2G q mean	$\mathcal{U}(0, 1)$
σ_q	1G+2G q width	$\mathcal{U}(0.02, 1)$
$\mu_{\chi_{\text{eff}}}$	1G+1G χ_{eff} mean	$\mathcal{U}(-0.3, 0.3)$
$\sigma_{\chi_{\text{eff}}}$	1G+1G χ_{eff} width	$\mathcal{U}(0.02, 0.3)$
μ_{χ_p}	1G+1G χ_p mean	$\mathcal{U}(0, 0.5)$
σ_{χ_p}	1G+1G χ_p width	$\mathcal{U}(0.02, 0.4)$
χ_c	1G+2G characteristic spin	$\mathcal{U}(0.3, 1)$
q_c	1G+2G characteristic mass ratio	$\mathcal{U}(0, 1)$
$\ln \sigma$	1G+2G ellipse width	$\mathcal{U}(-4, -1)$

TABLE I. Priors on the model parameters, separated by model component. For the branching fraction, we use either the constant ξ or the spline f_i .

We model the spline using 10 equally-log-spaced nodes between $m_1 = 2M_\odot$ and $m_1 = 200M_\odot$. Other numbers of nodes produce no tangible differences in results and 10 nodes has the best evidence. The latent values of the spline nodes are sampled from independent normal distributions $\mathcal{N}(0, 2)$ and are transformed to the unit interval with a sigmoid. All priors are given in Tab. I.

Additional results and model variations

Theoretical models for the 1G+2G mass ratio distribution find a peak near $q = 0.5$ [69, 70, 97]; as such, we separately model the 1G+1G and 1G+2G mass ratio distributions with results in Fig. 4, where 1G+1G is in solid teal and 1G+2G in dashed pink. While the 1G+2G result is shifted away from unity vis-à-vis the 1G+1G distribution, the hyperparameters μ_q and σ_q are poorly constrained, indicating the data are not sufficiently in-

formative about the mass ratio distribution of the hierarchical component.

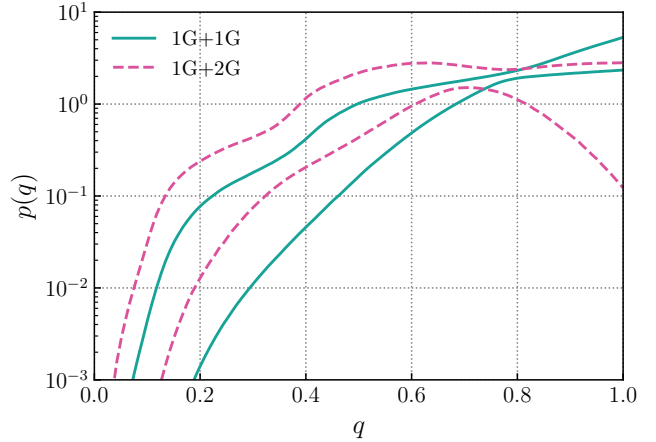


FIG. 4. The 90% credible bounds on the marginal mass ratio distributions for the first-generation component (solid teal), modeled by a truncated power law, and the hierarchical component (dashed pink), modeled with a truncated normal.

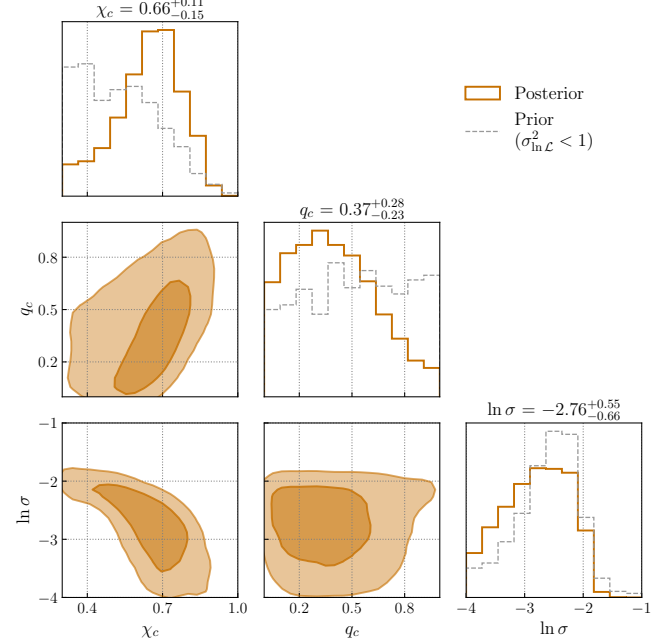


FIG. 5. Marginal and two-dimensional joint posteriors on the characteristic spin χ_c , characteristic mass ratio q_c , and width $\ln \sigma$ of the ellipse component. The dashed gray histograms in the marginals consist of draws from the prior that pass the likelihood variance cut.

The posteriors on the ellipse parameters—characteristic spin χ_c , characteristic mass ratio q_c , and width $\ln \sigma$ —are in Fig. 5. The positive correlation between χ_c and q_c arises from their inverse effects on the width of the marginal χ_{eff} distribution. We confirm

through a leave-one-out analysis that these results are not driven solely by the exceptional event GW231123, which may possess near-extremal spins. Including GW231123 narrows the ellipse in χ_{eff} (increases q_c) and raises it in χ_p (increases χ_c), but results are consistent to well within uncertainty.

The inferred low-mass subpopulation does not entirely depend on GW241011 and GW241110. Excluding these events, the location of the peak remains centered at $m_{\text{peak}} = 15.7 M_\odot$, but the inferred fraction of hierarchical mergers at m_{peak} is reduced from $\xi(m_{\text{peak}}) = 0.57^{+0.31}_{-0.37}$ to $\xi(m_{\text{peak}}) = 0.37^{+0.46}_{-0.31}$. In Fig. 6 we show the inference on $\xi(m_1)$ using all 155 events (solid red), excluding GW241011 and GW241110 (dashed blue), and excluding GW231123 (dotted black).

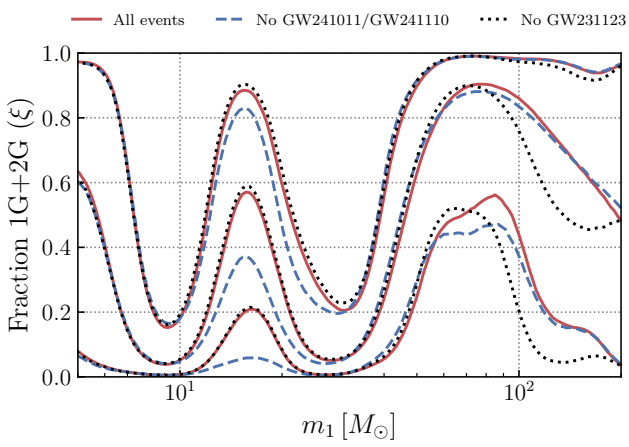


FIG. 6. The fraction of hierarchical mergers $\xi(m_1)$. In red, we analyze all 153 events in O4a alongside GW241011 and GW241110. In dashed blue, we only analyze the 153 O4a events. In dotted black, we include GW241011 and GW241110 but exclude GW231123.

We also test skew-normal and correlated models for the 1G+1G population, as recently employed by the LVK [5, 12, 121], and find both are *disfavored* over a Gaussian 1G+1G component. The posteriors on the skewness and correlation coefficient are centered near and consistent with zero. This suggests the inferred skewness in Ref. [5] comes from a need to accommodate a dominant population with primarily positive χ_{eff} and a sub-dominant group that includes negative χ_{eff} . However, a two-component model with a symmetric, narrow dominant component better fits the data.

The results presented above enforce symmetry in the

ellipse component about $\chi_{\text{eff}} = 0$. We test whether this assumption is valid by allowing the ellipse to be non-centered in χ_{eff} . The posterior on the centering parameter χ_0 is slightly positive, but consistent with zero, and the non-centered model is mildly disfavored over a centered ellipse. The preference for symmetry suggests hierarchical mergers from dense stellar clusters, as opposed to AGN or triple systems, dominate the population.

Individual-event Bayes factors

We compute the Bayes factor for each event to come from the 1G+2G over the 1G+1G component both for the constant ξ and evolving $\xi(m_1)$ models as

$$\mathcal{B}_{1G+1G}^{1G+2G}(n) = \frac{p(G_n = 1G + 2G | \{d\})}{p(G_n = 1G + 1G | \{d\})}, \quad (8)$$

where G_n is the generation of the n^{th} event, and the marginal posterior on generation is

$$p(G_n | \{d\}) = \int d\Lambda d\theta_n p(\Lambda | \{d\}) p(G_n | \Lambda) \quad (9)$$

$$\times p(\theta_n | G_n, \Lambda) \frac{p(\theta_n | d_n)}{p(\theta_n)} \frac{p(d_n)}{p(d_n | \Lambda)}. \quad (10)$$

The normalization term $p(d_n | \Lambda) / p(d_n) = \int d\theta p(\theta | d_n) p(\theta | \Lambda) / p(\theta)$. In practice, these integrals are computed with Monte Carlo sums over individual-event samples θ and hyperposterior samples Λ .

For the constant- ξ model, the events with the highest Bayes factors are GW241011 ($\ln \mathcal{B} = 7.6$), GW190517 ($\ln \mathcal{B} = 4.1$), GW231028_153006 ($\ln \mathcal{B} = 3.15$), and GW241110 ($\ln \mathcal{B} = 2.5$). GW231123 is ranked sixth. The same events are top-ranked under the evolving $\xi(m_1)$ model: GW241011 ($\ln \mathcal{B} = 10.5$), GW231028_153006 ($\ln \mathcal{B} = 6.3$), GW190517 ($\ln \mathcal{B} = 3.6$), and GW241110 ($\ln \mathcal{B} = 3.6$). GW231123 is ranked eighth; its lower significance in the evolving model may arise from the measurement of ξ broadening toward the prior at masses as high as its primary mass, $\sim 120 M_\odot$. Several of these candidates overlap with those identified in other works [e.g. 45, 92]. In a companion paper [102], we use a machine-learning-based cluster simulation emulator to infer the host cluster properties of the events with the highest Bayes factors to come from the 1G+2G components, as well as the events with the highest χ_p likelihood ratios, a classification metric introduced by [96].